Nuclear Instruments and Methods in Physics Research A 699 (2013) 235–241

Contents lists available at SciVerse ScienceDirect

Nuclear Instruments and Methods in Physics Research A

journal homepage: www.elsevier.com/locate/nima

A novel gamma-ray detector with submillimeter resolutions using a monolithic MPPC array with pixelized Ce:LYSO and Ce:GGAG crystals

T. Kato [a,*], J. Kataoka [a], T. Nakamori [a], T. Miura [a], H. Matsuda [a], A. Kishimoto [a], K. Sato [b], Y. Ishikawa [b], K. Yamamura [b], S. Nakamura [b], N. Kawabata [b], H. Ikeda [c], S. Yamamoto [d], K. Kamada [e]

[a] Research Institute for Science and Engineering, Waseda University, 3-4-1, Ohkubo, Shinjuku, Tokyo, Japan
[b] Solid State Division, Hamamatsu Photonics K. K., 1126-1, Ichino-cho, Hamamatsu, Shizuoka, Japan
[c] ISAS/JAXA, 3-1-1, Yoshinodai, Chuo-ku, Sagamihara-shi, Kanagawa, Japan
[d] Kobe City College of Technology, 8-3, Gakuenhigashimati, Nishi-ku, Kobe-shi, Hyougo 651-2194, Japan
[e] Materials Research Laboratory, Furukawa Co., Ltd., 1-25-13, Kannondai, Tsukuba, Ibaraki 305-0856, Japan

ARTICLE INFO

Available online 26 April 2012

Keywords:
Multi-pixel photon counter
Gamma-rays
Positron emission tomography

ABSTRACT

We have developed a large-area monolithic Multi-Pixel Photon Counter (MPPC) array consisting of 4×4 channels with a three-side buttable package. Each channel has a photosensitive area of 3×3 mm^2 and 3600 Geiger mode avalanche photodiodes (APDs). For typical operational gain of 7.5×10^5 at $+20$ °C, gain fluctuation over the entire MPPC device is only $\pm 5.6\%$, and dark count rates (as measured at the 1 p.e. level) amount to ≤ 400 kcps per channel. We first fabricated a gamma-ray camera consisting of the MPPC array with one-to-one coupling to a Ce-doped (Lu, Y)$_2$(SiO$_4$)O (Ce:LYSO) crystal array (4×4 array of $3 \times 3 \times 10$ mm^3 crystals). Energy and time resolutions of $11.5 \pm 0.5\%$ (FWHM at 662 keV) and 493 ± 22 ps were obtained, respectively. When using the charge division resistor network, which compiles signals into four position-encoded analog outputs, the ultimate positional resolution is estimated as 0.19 mm in both *X* and *Y* directions, while energy resolution of $10.2 \pm 0.4\%$ (FWHM) was obtained. Finally, we fabricated submillimeter Ce:LYSO and Ce-doped $Gd_3Ga_3Al_2O_{12}$ (Ce:GGAG) scintillator matrices each consisting of 1.0×1.0, 0.7×0.7 and 0.5×0.5 mm^2 pixels, to further improve the spatial resolution. In all types of Ce:LYSO and Ce:GGAG matrices, each crystal was clearly resolved in the position histograms when irradiated by a ^{137}Cs source. The energy resolutions for 662 keV gamma-rays for each Ce:LYSO and Ce:GGAG scintillator matrix were $\leq 14.3\%$. These results suggest excellent potential for its use as a high spatial medical imaging device, particularly in positron emission tomography (PET).

1. Introduction

Positron emission tomography (PET) imaging is a well-established method of detecting cancers and diagnosing Alzheimer's in its early stages [1]. Currently, many advantageous aspects of PET combined with Magnetic Resonance Imaging (MRI) (MRI–PET) are being proposed, and with prototypes now being tested as MRI produces an excellent soft-tissue contrast and anatomical detail without additional radiation [2–4]. However, the Photo-Multiplier Tube (PMT) incorporated in conventional PET scanners is difficult to use within the high magnetic field of MRI. Moreover, the large-size PMT-based on PET not only complicates use in narrow MRI tunnels but also limits the spatial resolution far from the theoretical limit of PET resolution. One approach to solving this problem is using the avalanche photodiode (APD) a compact type of semiconductor photodetector. Various PET modules utilizing APDs have successfully demonstrated the potential for simultaneous MRI–PET imaging [5] as well as ultimate submillimeter spatial resolution [6]. One disadvantage of using APDs is the relatively low avalanche gain (typically ≤ 100), which means that APDs easily affected by electric noise contamination; moreover, APDs always require a Charge Sensitive Amplifier (CSA) that critically limits time resolution [7].

The Multi-Pixel Photon Counter (MPPC), also known as a Silicon Photo-Multiplier (SiPM), is a compact type of high performance semiconductor photodetector consisting of multiple Geiger-mode APD pixels. One [8] summarizes the principles of operation and basic performance the MPPC. The MPPC offers many advantages like the APDs described above, such as its insensitivity to magnetic fields and compactness. In addition, it is operated in Geiger-mode, resulting in gain comparable to that of PMTs at up to the 10^5–10^6 level. Despite its superior

* Corresponding author.
E-mail address: katou.frme.8180@asagi.waseda.jp (T. Kato).

0168-9002/$ - see front matter © 2012 Elsevier B.V. All rights reserved.
http://dx.doi.org/10.1016/j.nima.2012.04.008

advantages, however, the MPPC also has several weak points compared to traditional PMTs and APDs. First, the number of Geiger-mode APD pixels that comprise the MPPC limits its dynamic range. Once Geiger-discharge has been triggered, each of pixel is subject to dead time (typically measured in tens of ns) during which multiple photons entering a single pixel cannot be counted, resulting in a nonlinear response to the number of incident photons. Secondly, thermal electrons also trigger a Geiger-discharge, resulting in a substantial contamination of dark counts. Nevertheless, its great advantages make the MPPC an ideal photosensor for MRI–PET as well as for Time Of Flight (TOF) applications [9–12].

A high-resolution MRI–PET/TOF–PET technique utilizing the MPPC array is now being developed. We previously developed and tested a large-area, monolithic 4×4 MPPC array [13]. In this paper, we report the performance of a newly designed monolithic 4×4 MPPC array used as a gamma-ray detector [14]. The MPPC array is characterized by its quite small three-side buttable package, where the gap between each MPPC array can be minimized when arrays are arranged flush against each other. To fabricate a gamma-ray detector, we selected Ce-doped $(Lu,Y)_2(SiO_4)O$ (Ce:LYSO) with a brand-new scintillator, Ce-doped $Gd_3Ga_3Al_2O_{12}$ (Ce:GGAG) due to their high light yield and short scintillation decay time [15,16].

This paper is organized as follows: Section 2 presents the performance of the MPPC array together with Ce:LYSO scintillator matrix. Section 3 describes the resistor network readout circuit we applied to reduce the number of readouts, and our successful event reconstruction of interaction positions and energies for gamma-rays. Section 4 describes our fabrication and testing of a PET detector module using submillimeter Ce:LYSO and Ce:GGAG scintillator matrices, and the resistor network. We achieved pixel identification in flood images. Section 5 presents our final conclusions.

2. Performance of the MPPC array

The monolithic 4×4 MPPC array described here was designed and developed for future applications in nuclear medicine (such as PET scanners) by Hamamatsu Photonics K.K. (Fig. 1). Each channel has a photosensitive area of 3×3 mm^2 and 60×60 Geiger mode APDs arranged with a pitch of 50 μm. The gap between each channel is only 0.2 mm thanks to the monolithic structure. The MPPC array is placed on a surface-mounted package measuring 14.3 by 13.6 mm, and fabricated into a three-side buttable structure, that is, the distance from the photosensitive area to the edge of the package is a mere 500 μm. Signals from individual channels can be read through a flexible printed circuit (FPC) cable that easily connects the MPPC array to subsequent electronic circuits. The average gain of the MPPC array was 7.5×10^5 at voltage of 72.01 V, and fluctuation in gain was only $\pm5.6\%$ over 4×4 MPPC channels as measured at $+20$ °C. The dark count rates due to the

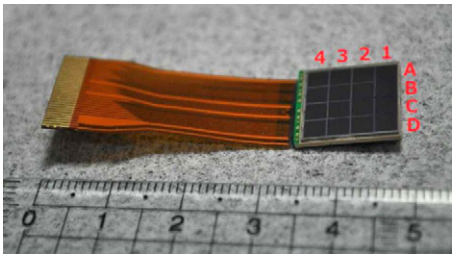

Fig. 1. Photo of the 4×4 MPPC array developed in this paper. Numbers 1–4 and the letters A to D identify the channels of the MPPC array.

Table 1
Specification of the 4×4 MPPC array at $+25$ °C.

Parameters	Specification
Number of elements (ch)	4×4
Effective active area/channel (mm)	3×3
Pixel size of a Geiger-mode APD (μm)	50
Number of pixels/channel	3600
Typical photon detection efficiency[a] ($\lambda=440$ nm) (%)	50
Typical dark count rates/channel (kcps)	≤400
Terminal capacitance/channel (pF)	320
Gain (at operation voltage)	7.5×10^5

[a] Including cross-talk and after-pulse contributions.

Table 2
Basic characteristics of the Ce:LYSO and Ce:GGAG scintillators.

Parameters	Ce:LYSO	Ce:GGAG
Density (g/cm^3)	7.10	6.63
Light yield (photons/MeV)	25,000	42,000
Decay time (ns)	40	52.8 (73%) and 282 (27%)
Peak wavelength (nm)	420	520

1 p.e. level was about 300–400 kcps per pixel, which was much less than that of conventional MPPCs [17]. Table 1 lists the other basic characteristics of the MPPC array.

We fabricated a Ce:LYSO scintillator array to be coupled with the MPPC array. This Ce:LYSO array has geometry precisely matching that of the MPPC array, that is, a 4×4 array of $3\times3\times10$ mm^3 pixels, and a 0.2 mm gap between them. Each scintillator pixel is divided with a reflective $BaSO_4$ layer 0.2 mm thick. Table 2 lists the basic parameters of Ce:LYSO. Silicon optical grease (OKEN 6262A) was used in optical coupling between the Ce:LYSO matrix and the MPPC array surface. Fig. 2 shows the energy spectra measured with a ^{137}Cs source corrected for non-linearity. The linearity correction is discussed in detail in Ref. [13]. The averaged energy resolution for the 662 keV photoelectric peak was $11.5\pm0.5\%$ (FWHM) over 4×4 MPPC channels.

The time resolution of the MPPC array coupled with the Ce:LYSO matrix was then measured against a PMT (Hamamatsu R 7899-MOD1 (EG)) coupled with a $3\times3\times10$ mm^3 crystal of the Ce:LYSO scintillator. The PMT and MPPC array were set at back-to-back positions. The distance between both detectors was about 30 mm, and a ^{22}Na point source was placed near the center. The output signal from the PMT was fed into a constant fraction discriminator (ORTEC 935; hereafter CFD) and its output was used to generate start input on a time-to-amplitude converter (ORTEC 567; hereafter TAC). The output signals form the MPPC array were fed into the CFD with a fixed delay to generate stop input on the TAC. TAC output was then fed into the peak hold ADC (CLEAR PULSE 1113A; hereafter PHADC). To select the events of 511 keV annihilation quanta, the gate of PHADC was activated by the coincidence of the PMT and the MPPC array output signals, as determined by using a coincidence module (Technoland N-TM 103). Fig. 3 shows the results. The time resolution of 493 ± 22 ps (FWHM) was obtained over 4×4 MPPC channels.

3. Charge division readout technique

When our previously described detectors are integrated as a complete PET scanner, the large number of channels is likely to

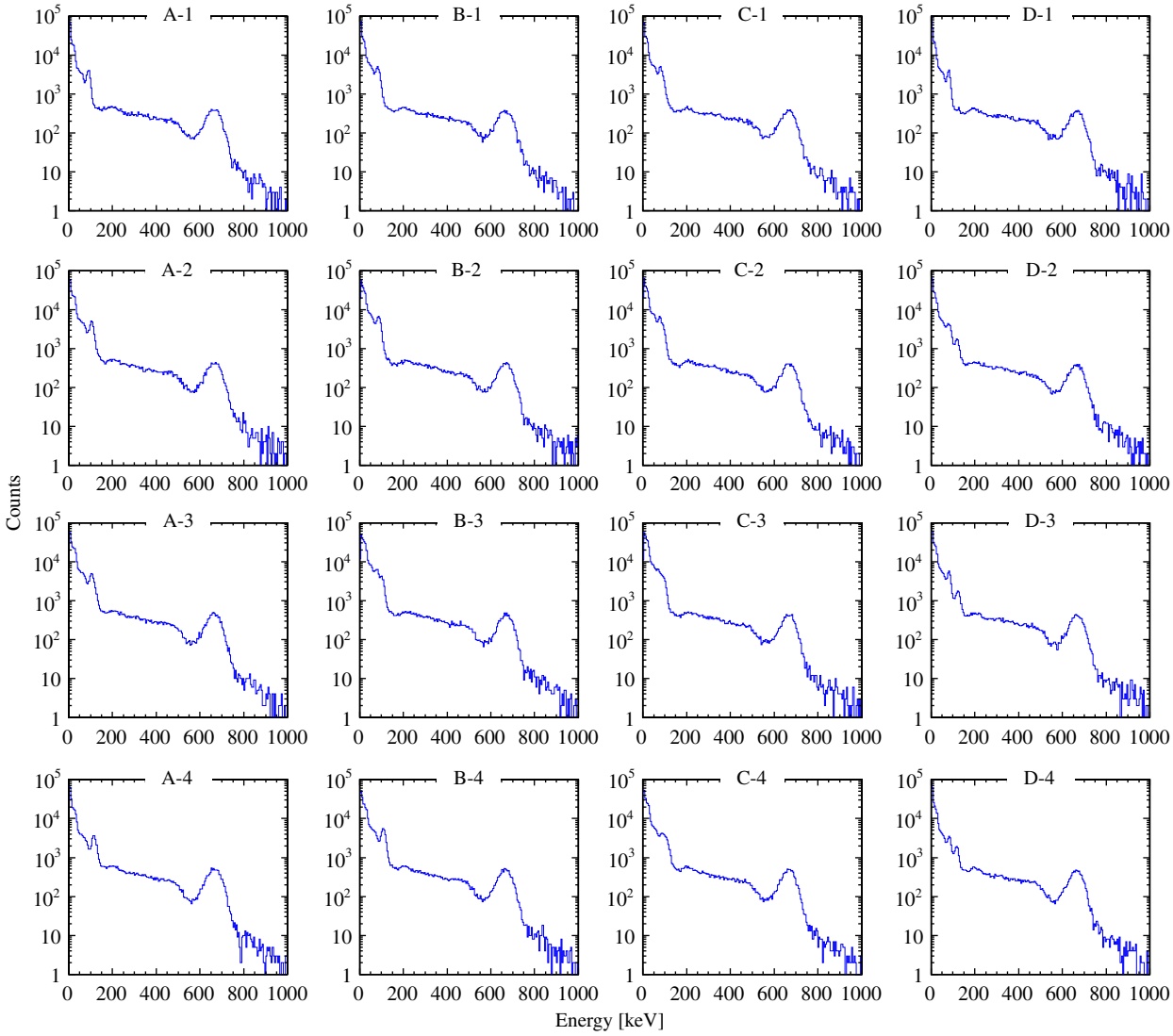

Fig. 2. Energy spectra of ^{137}Cs source coupled with the Ce:LYSO matrix on the MPPC array for all pixels at 72.01 V at +20 °C.

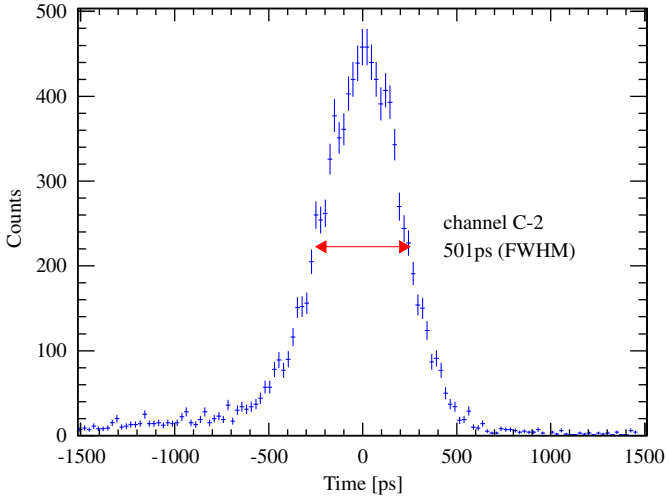

Fig. 3. Time distribution of the MPPC array's response to the PMT for channel C-2.

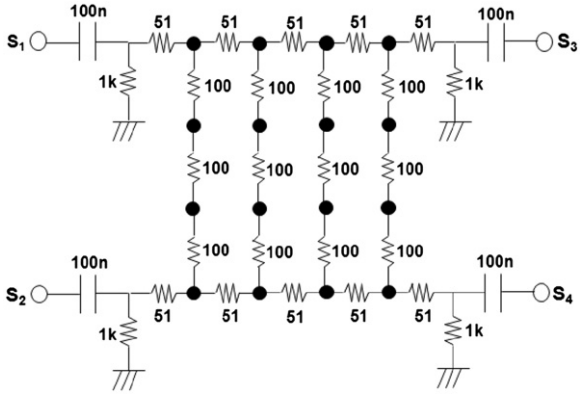

Fig. 4. Diagram of the charge division resistor network. 16 anodes of the MPPC array are directly connected to the filled circles. The units of value are Ω and F for resistor and capacitor, respectively.

prove problematic. Since larger readout electronics are required, along with the number of detector channels, costs, power consumption and equipment size would all diverge. We responded by applying a charge division readout technique a well-established method for multi-anode PMTs [18,19] that is sometimes applied for MPPCs [20]. Fig. 4 shows the resistor

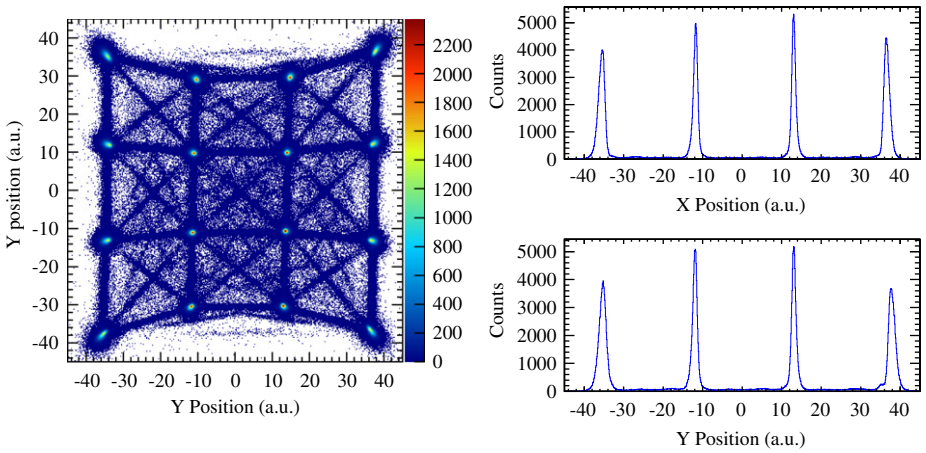

Fig. 5. *left*: Flood image of 4×4 Ce:LYSO matrix measured with a ^{137}Cs source. *X* and *Y* positions indicate the direction from A to D and from 4 to 1 channel in Fig. 1, respectively. *right*: A count profile in the *X* direction from the bottom row (*top*) and *Y* direction from the left column (*bottom*) in the flood image.

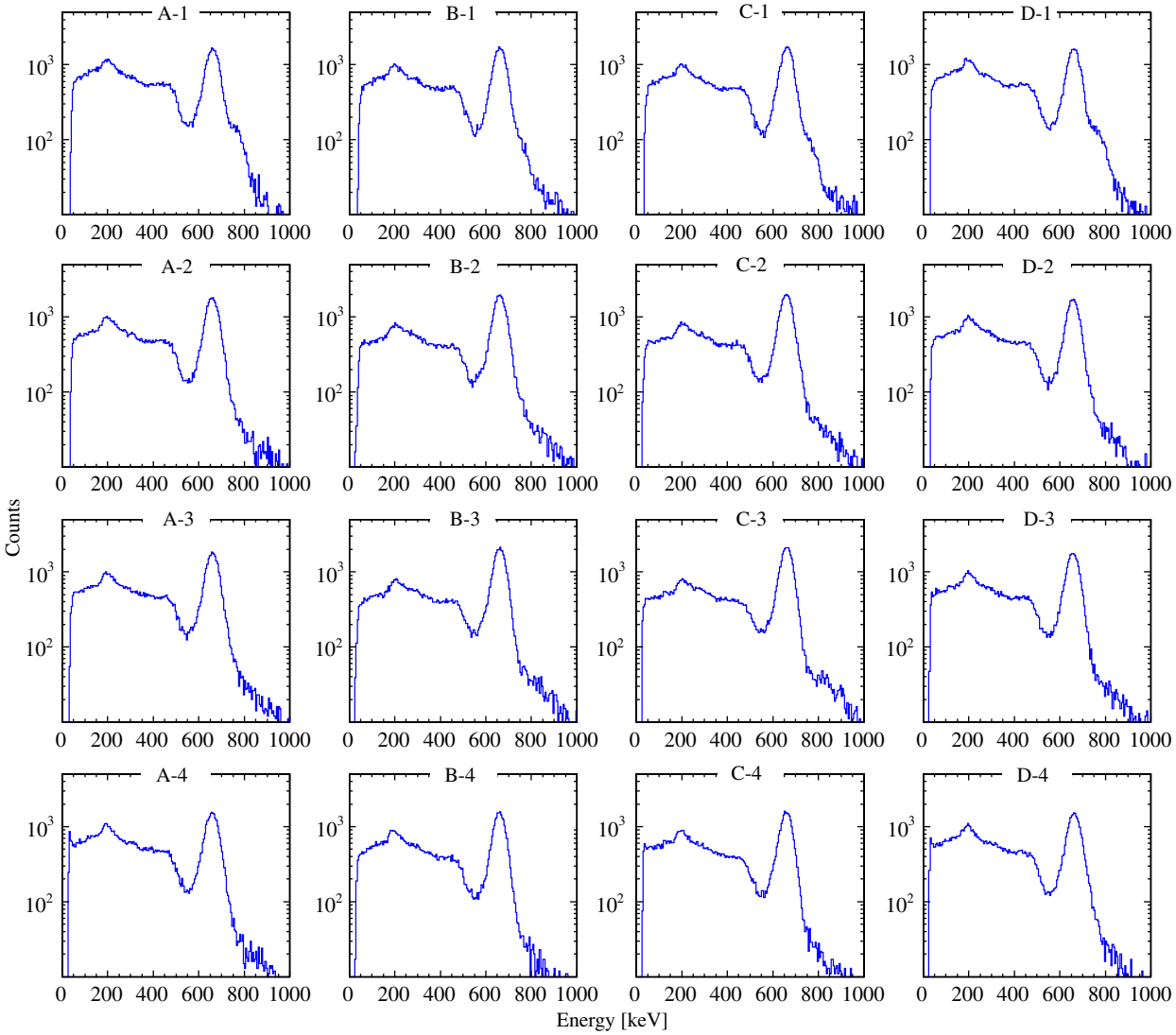

Fig. 6. Energy spectra of a ^{137}Cs source reconstructed from the flood image.

network we used to compile signals into four position-encoded analog outputs in our experiments. The sum of the four output signals corresponded to the total energy deposition of the gamma-ray, with the *x* and *y* interaction positions being calculated by using the centroid method, that is, the following equation:

$$X = (S_3 + S_4 - S_1 - S_2)/(S_1 + S_2 + S_3 + S_4) \quad (1)$$

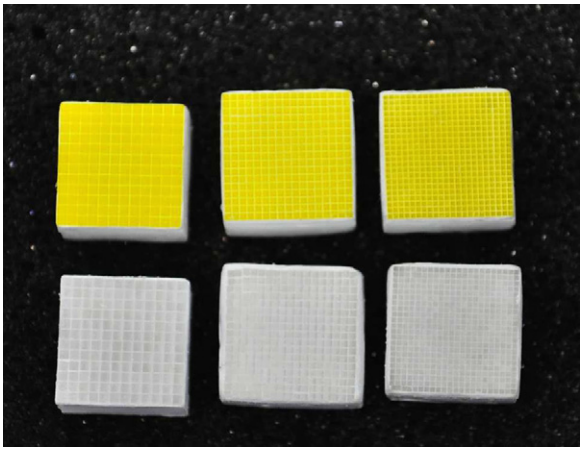

Fig. 7. Photos of the submillimeter pixelized scintillator matrices to be coupled with the MPPC array. Ce:GGAG and Ce:LYSO matrices are presented in the top and bottom rows, respectively. (From left to right: 12×12, 17×17 and 22×22 matrices of 1.0×1.0, 0.7×0.7 and 0.5×0.5 mm^2 pixels).

$$Y=(S_1+S_3-S_2-S_4)/(S_1+S_2+S_3+S_4) \quad (2)$$

where S_1 denotes the charge recorded from the channel as shown in Fig. 4.

The four signals from the resistor network were fed into Quad Linear FAN IN/OUT (Phillips MODEL 6954) and divided into two lines. One was directly fed into the charge-sensitive ADC (HOSHIN V005; hereafter CSADC), with the other being summed over four signals to generate a trigger with the non-update discriminator (Technoland N-TM 405). The gate width of the CSADC was set to 700 ns. We used the resistor network to evaluate flood images and energy resolution. These measurements were conducted at bias voltage of 72.01 V at $+20$ °C.

First, a ^{137}Cs source was used to acquire a 2D position histogram and verify pixel separations. Fig. 5(*left*) shows the flood image results. Although the outer pixels tend to have broader peaks, all pixels were clearly resolved. Fig. 5(*right*) shows the projection of the bottom row and left column. The reconstructed position is calibrated to match the actual detector dimensions, whereupon the averaged FWHM

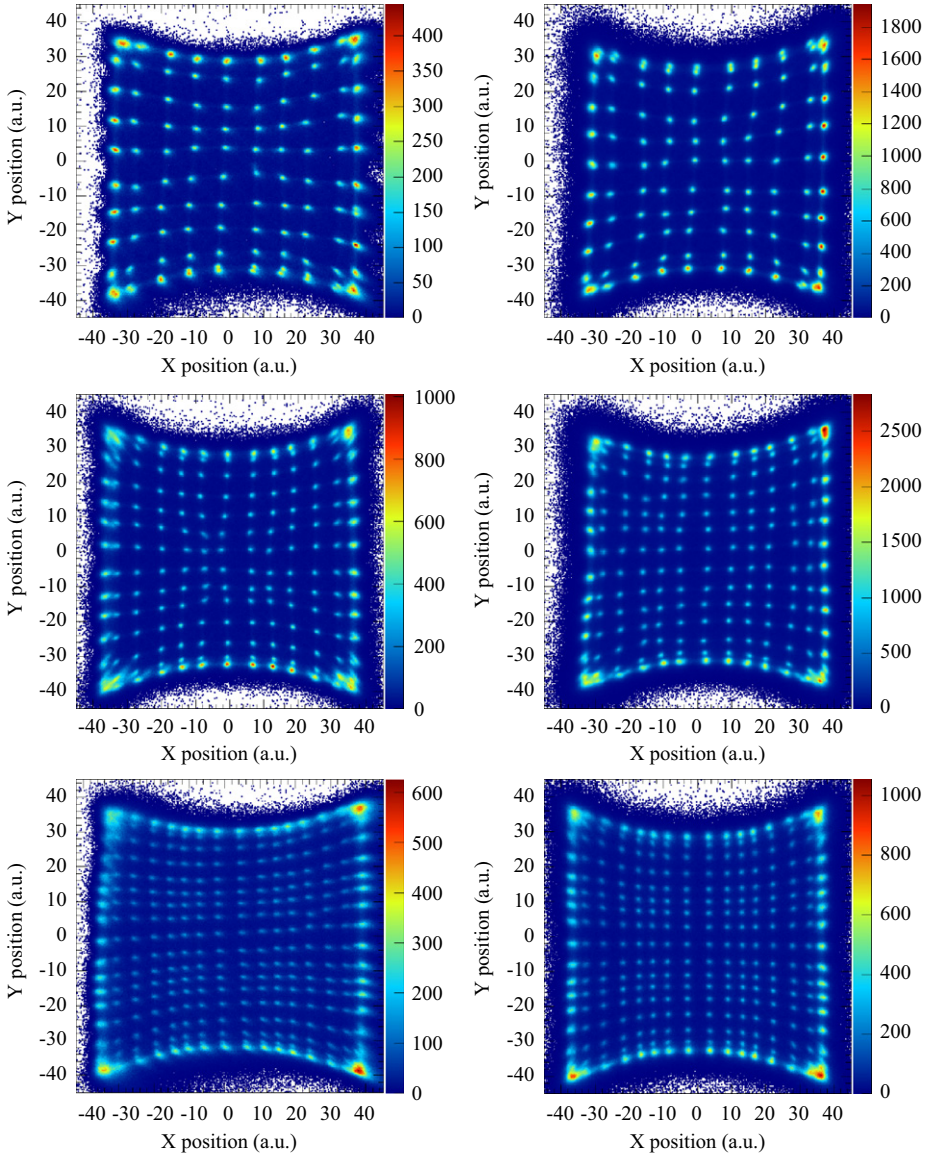

Fig. 8. Flood images of each submillimeter scintillator matrix as measured with a ^{137}Cs source. Left and right columns show the flood images of Ce:LYSO and Ce:GGAG, respectively. From top to bottom, 12×12, 17×17 and 22×22 arrays of 1.0×1.0, 0.7×0.7 and 0.5×0.5 mm^2 pixels are presented, respectively.

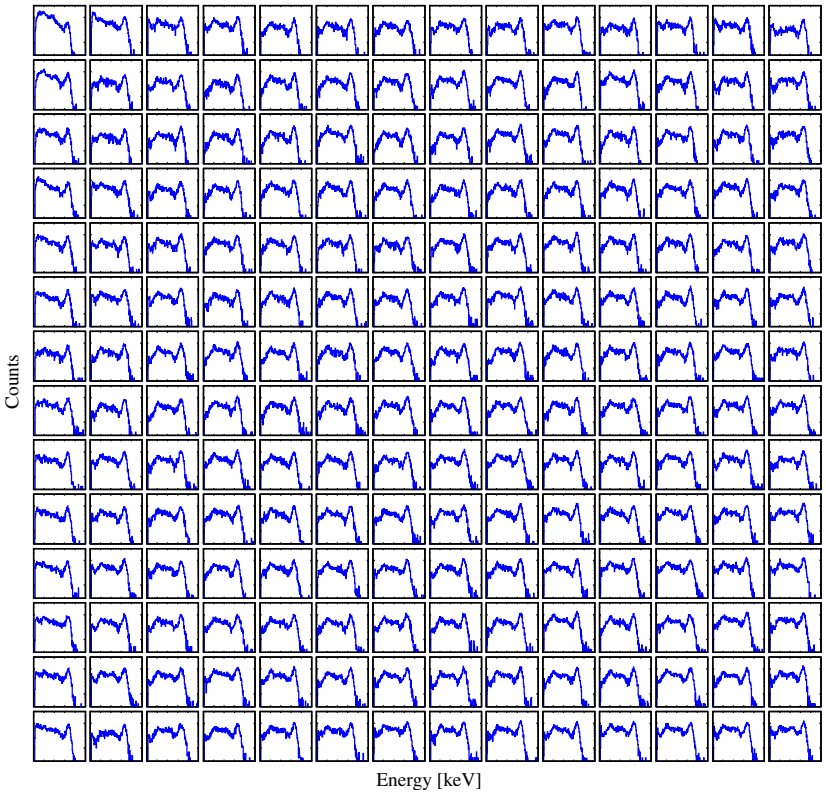

Fig. 9. Energy spectra of a ^{137}Cs source for 0.5 mm^2 Ce:LYSO matrix reconstructed from the flood image.

Table 3
Averaged energy resolution (FWHM) for 662 keV photoelectric peak for each submillimeter scintillator matrices.

Pixel size of scintillator matrices (mm^2)	Ce:LYSO	Ce:GGAG
1.0×1.0	11.5 ± 0.9	9.1 ± 0.8
0.7×0.7	11.7 ± 0.7	10.4 ± 1.2
0.5×0.5	14.3 ± 1.8	12.0 ± 1.3

of all peaks were obtained as 0.19 mm in both X and Y directions.

We then extracted energy spectra from all pixels by selecting events around the corresponding peak in the flood image. Fig. 6 shows ^{137}Cs gamma-ray spectra after linearity correction. The averaged energy resolution for the 662 keV photoelectric peak was $10.2 \pm 0.4\%$ (FWHM), or slightly better than when using the discrete readout system. This is probably because the resistor network could collect all the charges generated, even if scintillation photons are leaking to neighboring pixels. The greater the charges involved, naturally, the better the energy resolution.

4. Performance with submillimeter pixelized scintillator matrices

To further improve the spatial resolution, we fabricated submillimeter Ce:LYSO and Ce:GGAG scintillator matrices, namely, 12×12, 17×17 and 22×22 matrices of 1.0×1.0, 0.7×0.7 and 0.5×0.5 mm^2 pixels for each, respectively (Fig. 7). Table 2 lists the basic parameters of Ce:GGAG. We noted that Ce:GGAG has a long decay time in contrast to Ce:LYSO, but its high light yield is beneficial in improving the signal-to-noise (S/N) ratio and energy resolution. Each scintillator pixel is divided with a reflective $BaSO_4$ layer 0.1 mm thick. The total size of the scintillator matrices are $13.1 \times 13.1 \times 10$ mm^3 for the 12×12 and 22×22 matrices, and $13.5 \times 13.5 \times 10$ mm^3 for the 17×17 matrix. These scintillator matrices were optically coupled to the MPPC array with an acrylic light guide 1 mm thick, which distributes scintillator photons across multiple MPPC array channels. Flood images and energy resolutions were evaluated for each scintillator matrix using the charge division readout technique, measured at 72.01 V at $+20$ °C. The measurements were set-up the same as for the experiments described in Section 3.

Fig. 8 shows flood image results obtained for each scintillator matrix by irradiating a ^{137}Cs source. The flood images show overlapping peaks of the side pixels, as the total size of scintillator matrices is a bit larger than the sensitive area of the MPPC array. And scintillation photons from the side pixels were only fed into the side channels of the MPPC array. However, the central pixels were successfully resolved in the flood images.

We extracted energy spectra from only resolved pixels by selecting events around the corresponding peaks in the flood images (Fig. 9). Table 3 lists the energy resolution results for the 662 keV photoelectric peak for each scintillator. The finer the scintillator pixel size, the worse the averaged energy resolution becomes. This is probably because the transfer of light from an interacting gamma-ray position to the MPPC array surface is accompanied by multiple scatterings on the $BaSO_4$ layer for a large height-to-bottom ratio of scintillator pixels. Increasing the number of reflections would reduce the scintillation photons

detected, therefore, energy resolution becomes worse. Meanwhile, Ce:GGAG shows better resolution than Ce:LYSO thanks to its large light yield.

5. Conclusion

In this paper, we report the results of a charge division readout technique using the 4×4 monolithic MPPC array which has fine gain uniformity of $\pm 5.6\%$ and very low dark count rates of ≤ 400 kcps as measured at $+20$ °C. One 4×4 Ce:LYSO scintillator matrix of individual $3 \times 3 \times 10\ \mathrm{mm}^3$ scintillator crystals was fabricated for coupling with the MPPC array. Flood images showed that the 4×4 scintillator pixels were clearly resolved, and the averaged FWHM of all peaks were obtained as 0.19 mm in both X and Y directions after calibration to the actual detector dimensions. The better energy resolution of $10.2 \pm 0.4\%$ (FWHM) was achieved with the resistor network, when compared to the discrete readout system. Next, in order to improve the spatial resolution, we fabricated submillimeter Ce:LYSO and Ce:GGAG scintillator matrices of 1.0×1.0, 0.7×0.7 and $0.5 \times 0.5\ \mathrm{mm}^2$ for each. The side pixels overlapped in the flood images, but the central pixels were successfully resolved. These results suggest that a large-area monolithic MPPC array coupled with submillimeter pixelized Ce:LYSO and Ce:GGAG matrices could be promising as a high spatial resolution gamma-ray device, particularly for medical imaging.

Acknowledgment

We thank an anonymous referee for his/her useful comments and suggestions to improve the manuscript.

References

[1] W.W. Moses, Nuclear Instruments and Methods A 471 (2001) 209.
[2] R.R. Raylman, et al., Nuclear Instruments and Methods A 569 (2006) 306.
[3] H. Peng, et al., Nuclear Instruments and Methods A 612 (2010) 412.
[4] S. Yamamoto, et al., Annals of Nuclear Medicine 24 (2010) 89.
[5] C. Woody, et al., Nuclear Instruments and Methods A 571 (2007) 102.
[6] J. Kataoka, et al., IEEE Transactions on Nuclear Science NS-57 (5) (2010) 2448.
[7] T. Nakamori, T. Kato, J. Kataoka, T. Miura, H, Matsuda, K. Sato, Y. Ishikawa, K. Yamamura, N. Kawabata, H. Ikeda, G. Sato, K. Kamada, Development of a gamma-ray imager using a large area monolithic 4×4 MPPC array for a future PET scanner, Journal of Instrumentation, submitted for publication.
[8] K. Yamamoto, et al., IEEE Transactions on Nuclear Science Conference Record N30-102 (2006) 1094.
[9] C.L. Kim, et al., IEEE Transactions on Nuclear Science NS-56 (5) (2009) 2580.
[10] S. Espa na, et al., Nuclear Instruments and Methods A 613 (2010) 308.
[11] A. Nassalski, et al., IEEE Transactions on Nuclear Science NS-57 (3) (2010) 1008.
[12] S. Yamamoto, et al., Physics in Medicine and Biology 55 (2010) 5817.
[13] T. Kato, et al., Nuclear Instruments and Methods A 638 (2011) 83.
[14] K. Sato, et al., IEEE Transactions on Nuclear Science Conference Record NSSMIC (2010) 243.
[15] I.G. Valais, et al., Nuclear Instruments and Methods A 569 (2006) 201.
[16] K. Kamada, et al., Crystal Growth and Design 11 (2011) 4484.
[17] K. Yamamoto, et al., IEEE Transactions on Nuclear Science Conference Record N24-292 (2007) 1511.
[18] S. Siegel, et al., IEEE Transactions on Nuclear Science NS-43 (3) (1996) 1634.
[19] S. Vecchio, et al., Nuclear Instruments and Methods A 569 (2006) 264.
[20] T.Y. Song, et al., Physics in Medicine and Biology 55 (2010) 2573.